Earth and Planetary Science Letters 312 (2011) 1–12

Contents lists available at SciVerse ScienceDirect

Earth and Planetary Science Letters

journal homepage: www.elsevier.com/locate/epsl

Formation timescales of large Martian valley networks

Monica R.T. Hoke [a,b,*], Brian M. Hynek [a,c], Gregory E. Tucker [c,d]

[a] Laboratory for Atmospheric and Space Physics, 392 UCB, University of Colorado, Boulder, CO 80309, USA
[b] Department of Astrophysical and Planetary Sciences, University of Colorado, Boulder, CO 80309, USA
[c] Department of Geological Sciences, University of Colorado, Boulder, CO 80309, USA
[d] Cooperative Institute for Research in Environmental Sciences, University of Colorado, Boulder, CO 80309, USA

ARTICLE INFO

Article history:
Received 29 April 2011
Received in revised form 28 September 2011
Accepted 29 September 2011
Available online xxxx

Editor: T. Spohn

Keywords:
Mars
valley
networks
hydrology
transport
timescale

ABSTRACT

Assessing timescales for formation of the ancient Martian valley networks is key to interpreting the early climate on Mars. We determined the likely formation times for seven of the largest ancient valley networks on Mars using the Darcy–Weisbach equation for average flow velocity, three different sediment transport models, and a range of input parameters to encompass possible formation conditions. With runoff rates similar to intense storms in arid regions on Earth, the minimum formation timescales of these Martian valley networks range from 10^5 to 10^7 yr, depending on the specific valley network. Shorter formation timescales require hurricane-scale flows that, if minimized with assumptions of continuous formation unlike even terrestrial rates, could complete large valley network formation in as little as 200 to 5000 yr, though this is not the preferred interpretation. While these results do not support impact-induced climate change as the sole mechanism for creating precipitation sufficient to incise the large valley networks, neither do they extend the amount of time required to form the networks beyond their range in age, consistent with hypotheses that valley incision was constrained to a relatively short period of Martian history near the Noachian–Hesperian boundary, approximately 3.6 to 3.8 Ga.

1. Introduction

The presence of valley networks across much of the ancient surface of Mars (e.g. Hynek et al., 2010), together with the locations and morphologies of the Martian deltas (e.g. Di Achille and Hynek, 2010) and ancient paleolakes (e.g. Fassett and Head, 2008a; Irwin et al., 2005a), provides strong evidence that the Martian surface environment was once capable of sustaining liquid water at the surface. Many of the largest Martian valley networks, with their meandering trunks, densely dendritic form, and tributaries that reach up to drainage divides, appear to have formed primarily from surface runoff of precipitated water (e.g. Craddock and Howard, 2002; Hoke and Hynek, 2009; Howard et al., 2005; Hynek and Phillips, 2003; Hynek et al., 2010). These same valley networks have crater densities that place their formation in the Late Noachian and Early Hesperian (~3.5–3.8 Ga) (Fassett and Head, 2008b; Hoke and Hynek, 2009), consistent with their formation during a period of enhanced fluvial erosion and incision on Mars (e.g. Craddock and Howard, 2002; Howard et al., 2005; Hynek and Phillips, 2001, 2003; Hynek et al., 2010). Sustained liquid water on the Martian surface requires a thicker and warmer atmosphere than exists there today, though it has remained unclear how long such conditions were needed to produce the valley networks.

The large Martian valley networks likely formed by similar processes as terrestrial river valleys (e.g. Craddock and Howard, 2002; Howard et al., 2005; Hynek and Phillips, 2001, 2003; Irwin et al., 2005b), typically by the gradual erosion of sediment through bed load, suspended load, and wash load processes (e.g. Komar, 1980; Milton, 1973). Numerous sediment transport equations and friction functions have been derived from first-order physical laws and calibrated with terrestrial data to incorporate the influence of particle size and density, surface roughness, flow turbulence, and gravitational acceleration (e.g. Meyer-Peter and Muller, 1948; Ribberink, 1998; van Rijn, 1984a,b), and some of these have been applied to Mars (e.g. Kleinhans, 2005; Komar, 1979, 1980; Wilson et al., 2004).

Often the Manning (1891) equation for depth- and width-averaged flow velocity is applied to Martian conditions by adjusting the empirical Manning coefficient with the difference in equatorial surface gravity between Earth and Mars (e.g. Goldspiel and Squyres, 1991; Irwin et al., 2005b; Komar, 1979), and, in some cases, by incorporating the differences in roughness predictors between different flow systems (e.g. Gioia and Bombardelli, 2002; Wilson et al., 2004). The modified Manning coefficients, however, are weakly dependent on flow depth, do not explicitly include gravity or bed roughness, assume bankfull flow, and produce flow velocities that can vary by over a factor of two (e.g. Kleinhans, 2005; Wilson et al., 2004). This results in sediment transport rates that vary significantly, thus creating large error in discharge rates

* Corresponding author at: Laboratory for Atmospheric and Space Physics, 392 UCB, University of Colorado, Boulder, CO 80309, USA. Tel.: +1 719 352 8367; fax: +1 303 492 6946.
E-mail address: Monica.hoke@colorado.edu (M.R.T. Hoke).

0012-821X/$ – see front matter © 2011 Elsevier B.V. All rights reserved.
doi:10.1016/j.epsl.2011.09.053

and calculated volumes of water required to carve Martian outflow channels and valley networks (e.g. Wilson et al., 2004).

An alternative to the Manning equation that is often overlooked in the planetary science community is the Darcy–Weisbach (D–W) equation (Silberman et al., 1963), which, unlike the Manning equation, maintains an explicit dependence on the acceleration due to gravity (g). In addition, whereas the Manning equation includes an implicit power–law scaling relationship between roughness and flow depth, the D–W equation allows greater flexibility in calculating roughness directly from flow depth (h) and median grain size (D_{50}) (e.g. Silberman et al., 1963). Both flow depth and grain size are important variables in determining flow velocity and can have significantly different values for various terrestrial systems and, likewise, Martian flows. Therefore the D–W equation and the included friction function are better suited for modeling flows associated with sediment transport on Mars (e.g. Kleinhans, 2005; Komar, 1979; Wilson et al., 2004).

Additionally, some planetary researchers rely on empirical relationships between flood discharge (Q) and width (w) (e.g. Osterkamp and Hedman, 1982) to estimate the amount of water that carved the Martian valley networks (e.g. Irwin et al., 2005b). However, many of the Martian valley networks do not likely follow the empirical scaling relationships between width, slope, and area that are used for perennial channels on Earth (Som et al., 2009). With the improved topographic data now available for measuring volume, slope, and depth, Martian sediment transport can be better estimated with the less-empirical, more physically-based equations by Ribberink (1998), Meyer-Peter and Mueller (Wong and Parker, 2006), van Rijn (1984a), and others.

In this work, we investigate the formation timescales of the Martian valley networks through the use of three different sediment transport models, the D–W equation, and a variety of parameters to encompass a range of possible formation conditions. This is done specific to each of seven of the largest valley networks in the Terra Sabaea, Arabia Terra, and Meridiani regions of Mars (Fig. 1, Table 1). With total valley lengths that range from about 5000 km to 15,000 km, these valley networks represent some of the largest and most mature valley network systems on Mars. All of the valley networks in this study have dendritic branching patterns with drainage densities comparable to terrestrial values (e.g. Carr and Chuang, 1997; Hoke and Hynek, 2009; Hynek and Phillips, 2003). First-order tributaries within these networks reach up to drainage divides and interior valley dimensions increase downstream, consistent with their formation by precipitation (e.g. Hoke and Hynek, 2009). Crater-density analyses using techniques specific for narrow, linear features with limited surface area placed the end of formation for these valley networks at approximately 3.62 to 3.73 Ga (Hoke and Hynek, 2009) or 3.69 to 3.76 Ga (Fassett and Head, 2008b), all during the Late Noachian and Early Hesperian. Within this range of ages are valley networks that have distinctly separate ages and those that appear to be coeval (Hoke and Hynek, 2009). In some cases, the valley network morphologies and crater age dating indicate multiple periods of formation, including one network (Naktong Vallis) that has two branches (east and west) of distinctly different morphology and age (Hoke and Hynek, 2009).

To better represent past Martian conditions, we minimize the use of terrestrial empirical relationships, when possible. As well, we complete an analysis of an analogous terrestrial river system with the same methods. Finally, the valley network-specific sediment transport rates and formation timescales are compared with prior age-dating of the valley networks through crater density analysis (Hoke and Hynek, 2009) to understand the state of the climate at this time in Martian history.

2. Methods

To determine the formation timescales of the Martian valley networks using sediment transport models, three major variables are needed: the volume of sediment (V_s) removed during valley network formation; some measure of the distribution of grain sizes (D) that were presumably transported away during valley network formation; and the dimensions of the ancient river channels within the valleys that contained the flow. Many of these variables can be measured specific to the valley network and, when combined with a host of other minor variables (Table 2), provide valley network-specific paleo-discharges, sediment transport rates, and formation timescales.

2.1. Sediment volume

Volumes within the valleys were measured using ArcGIS software and Mars Global Surveyor (MGS) Mars Global Laser Altimeter (MOLA) topographic data (~463 m/pix) (Smith et al., 2001) and, where available, Mars Express High Resolution Stereo Camera (HRSC) topographic data (~75 m/pix) (Jaumann et al., 2007; Neukum et al., 2004). Valley topography was extracted using a mask that was manually drawn along the outer walls of the visible valleys from co-registered topographic data and Mars Odyssey (MO) Thermal Emission Imaging System (THEMIS) daytime infrared (IR) images (256 m/pix) (Christensen et al., 2004), and accounting for the local slope of the surrounding surface. It is assumed that infill of material since the end of valley network formation is negligible compared to the total volume

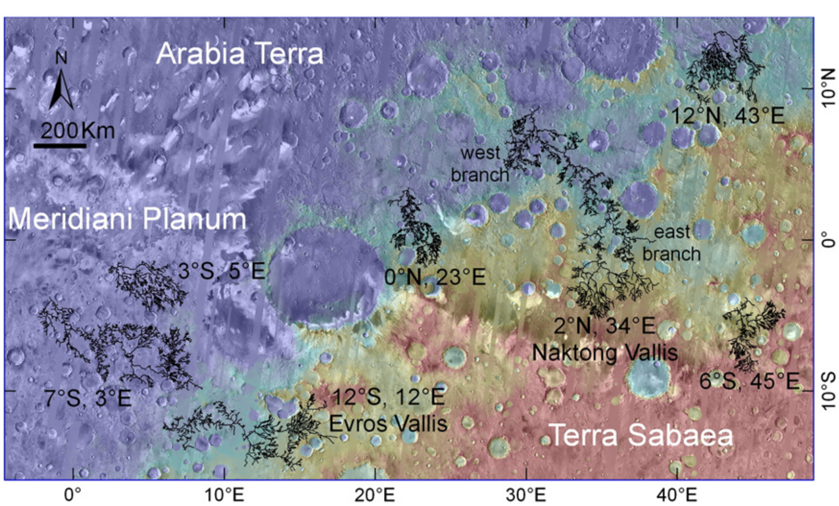

Fig. 1. The seven valley networks analyzed in this study (black lines) are shown with coregistered THEMIS daytime IR and MOLA topographic data.

Table 1
Valley network characteristics and ages (Hoke and Hynek, 2009).

Valley network	Stream length (km)	Drainage area (km^2)	Drainage density (km^{-1})	Approximate absolute age (Ga)
12°S, 12°E Evros	9050	149,700	0.060	3.63 ± 0.02
7°S, 3°E	11,710	148,300	0.079	3.65 ± 0.02
3°S, 5°E	5617	44,300	0.13	3.62 ± 0.03
0°N, 23°E	5389	43,400	0.12	3.68 ± 0.03
2°N, 34°E Naktong	15,265	286,800	0.053	3.72 ± 0.01
West branch	2563	22,200	0.12	3.79 ± 0.02
East branch	12,702	220,300	0.058	3.70 ± 0.01
12°N, 43°E	6463	69,700	0.093	3.73 ± 0.02
6°S, 45°E	4851	48,800	0.10	3.70 ± 0.02

of the valleys. The infill that undoubtedly has occurred has the effect of reducing the measured sediment volumes (V_s) from what actually may have been removed. Therefore, these volume estimates are minimum values that in turn correspond to minimum formation timescales.

2.2. Grain size

The distribution of rock sizes present during valley network formation is a very important variable in sediment transport calculations, but it also provides some of the greatest uncertainty in our results. For Mars, determining what grain size to use in calculating sediment transport is made especially difficult by the lack of direct measurements of the rock size distribution within the valleys during their formation due to their current inactive state and the accumulation of dust and sand (e.g. Carr and Malin, 2000) within the valleys over the last 3.6 to 3.8 Ga since the end of their formation (Hoke and Hynek, 2009). Using MGS Thermal Emission Spectrometer (TES) thermal inertia data (Putzig and Mellon, 2007) to determine grain size (e.g. Pelkey et al., 2001; Presley and Christensen, 1997) within these valleys produced median grain sizes of up to a few hundred micrometers in diameter, typical of sand. However, Christensen (1986) showed that the fine particle component of a surface dominates the thermal inertia values and thus thermal inertia values are unreliable for predicting particle size distributions on Mars, particularly for ancient features.

Rock size distributions from lander measurements provide an alternative to thermal inertia-derived grain sizes. Viking landers 1 and 2, the Pathfinder lander, and the Mars Exploration Rovers (MER) found rock size distributions to consist mostly of gravel and cobbles, 10 mm to 1 m in diameter, and sand, 0.1 mm to 2 mm in diameter (Fenton et al., 2003; Golombek et al., 2003, 2005, 2006; Herkenoff et al., 2004; Squyres et al., 2004). Converting the compiled rock size data (Wilson et al., 2004) from the Viking 1 and 2 landers and Pathfinder missions (Golombek and Rapp, 1997; Golombek et al., 2003) to a size-frequency distribution by mass rather than by number and accounting for kinematic sieving, Kleinhans (2005) determined a median grain size (D_{50}) value of 0.1 m. Although none of the lander-data compiled and analyzed by Kleinhans (2005) and Wilson et al. (2004) is from locations in or near valley networks, it is assumed that this rock distribution is typical of low latitude regions of Mars where these valley networks are found since all these surfaces have been similarly affected by impact gardening, aeolian processes, and other events that produced the rock size distribution we see today. Indeed, the MER rock size measurements (Golombek et al., 2005, 2006) produced similar distributions as other landers, though with fewer rocks and more sand at the Opportunity landing site in Meridiani Planum (Golombek et al., 2005; Squyres et al., 2004).

It should be noted that the 0.1 m median rock size determined by Kleinhans (2005) and used in this work has a large associated uncertainty since many processes may have modified the rocks since they were first emplaced (e.g. Carr, 1996; Fenton et al., 2003; Kleinhans, 2005). As well, limitations of the lander measurements, such as camera resolution, kinematic sieving, and shielding of smaller grains by larger cobbles, may result in inaccurate measurements that favor larger grain sizes (e.g. Kleinhans, 2005). Further, any differences in rock sizes between the southern highlands where most of the valley networks formed and the northern lowlands where most of the Martian landers are located may make the median grain sizes assumed in this work less applicable. Since the sediment transport calculations depend strongly on grain size, as discussed in following sections, the order of magnitude uncertainty in the 0.1 m median grain size is an important consideration. However, this is the best estimate at present and further refined estimates of surface rock size distributions will lead to more accurate formation timescales.

Table 2
Values of constants in Mars sediment transport equations.

Acceleration due to gravity(g)	3.71 m/s^2
Bed porosity (λ)	0.3
Sediment density (ρ_s)	3400 kg/m^3
Water density (ρ_w)	1000 kg/m^3
Kinematic viscosity (ν)	1.6×10^{-6} Pa•s
Von Karman constant (κ)	0.4
Critical Shields parameter (θ_{cr})	0.03

2.3. Channel dimensions

Measurements of the channel dimensions within the valleys nearest to the network outlet were preferred as they represent the space through which all upstream flow and sediment traveled. Channel slopes (s) were calculated with MOLA data along the lower 10% of the longest length profile of each valley network. This assumes that the channel slope is the same as the valley slope, which is a reasonable assumption given the uncertainty in these calculations.

Channel widths (w) were measured using 6 m/pixel resolution Mars Reconnaissance Orbiter (MRO) Context Camera (CTX) data (Malin et al., 2007), taking the width as being the distance across the channel perpendicular to the presumed direction of flow. Fig. 2 shows representative width measurements (in white) of the interior channel near the outlet of Naktong Vallis, along with corresponding cross-valley HRSC elevation profiles (in black). Channel width measurements for each valley network (Table 3) are averages of all channel measurements made near the outlet. Where no inner channels at the valley network outlet were visible, the average widths of the channels in other valley networks were used since the overall valley widths were similar. The measured channel widths interior to the valleys in this work are large compared to interior channel width measurements in other studies (e.g. Irwin et al., 2005b; Jaumann et al., 2005). However, the valley networks in this work are among the largest on Mars, and all measurements were made near the outlet where widths are expected to be greatest. Whereas, for example, the channel width measurements of ~450 +/− 50 m made by Jaumann et al. (2005) were from a valley network having a total length of 400 km, much smaller than the valley networks in this study (Table 1). Likewise,

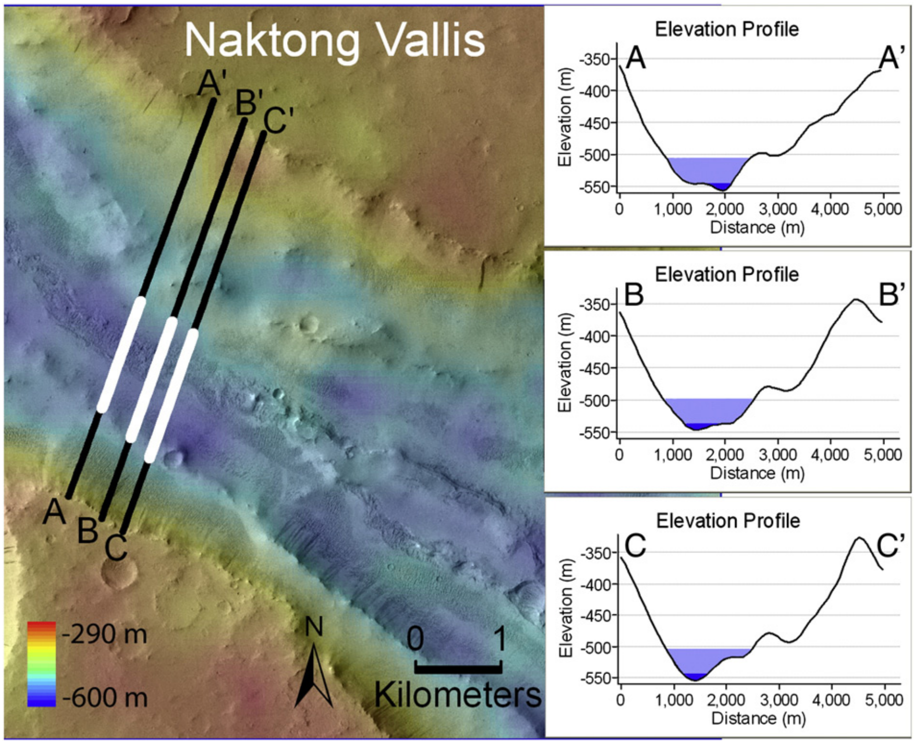

Fig. 2. Representative channel width measurements (white lines) and corresponding cross-valley elevation profiles (black lines and graphs) within Naktong Vallis near the outlet of the east branch. Width measurements across A, B, and C are 1.33 km, 1.55 km, and 1.34 km, respectively. Final width values in calculations for each valley network were averages of all measurements made within the network outlet area. Hypothetical depths of 10 m (dark blue fill) and 50 m (light blue fill) are shown in each elevation profile on the right. Image is co-registered CTX (P04_002758_1880_XI_08N329W) and HRSC data, centered at 7.5°N, 30.7°E. (For interpretation of the references to color in this figure legend, the reader is referred to the web version of this article.)

Irwin et al. (2005b) took interior channel measurements of 90 m to 1000 m from small valleys that were not necessarily located near the outlet of the respective network.

The depth of the flow (h) is a particularly important variable in sediment transport. Since the valley-incising flow depths of ancient rivers cannot be directly measured, they must be inferred from analysis of the interior channel morphology. The presence of terraces in MOLA and HRSC topographic data can provide a measure of bankfull depth, but this is made more difficult given the scarcity of identifiable channels where high-resolution topographic data (such as HRSC) exists and the obvious infilling by sand and dust as seen in high resolution images (such as CTX). Previously, researchers such as Goldspiel and Squyres (1991) used depths of 1 m, 5 m, 10 m, and 50 m in Martian discharge calculations. Others have measured depths of 25–55 m in Martian channels interior to other smaller valleys (Hauber et al., 2008; Jaumann et al., 2005). Measurements with HRSC data over Naktong Vallis based on identifying terraces within the ancient river channel provided depths of 31 +/− 12 m. Due to the uncertainty in depth estimates, we maintain a range of depths between 1 m and 50 m in all calculations.

In an effort to more tightly constrain probable flow depths specific to each valley network, we also calculated flow depth using two methods. A width-to-depth ratio of 58 based on terrestrial river dimensions for gravel river beds (Finnegan et al., 2005) and averaged parameters from satellite data (Bjerklie et al., 2003) resulted in Martian flow depths between 24 and 40 m, depending on the valley network. The applicability of this empirical relationship to ancient Martian rivers, however, is highly uncertain, and so it is used here simply as a guide for identifying possible flow depths.

Alternatively, flow depth was also estimated by setting the mean shear stress of the flow (τ) equal to 120% of the critical shear stress (τ_{cr}) required for sediment transport. This can be assumed for rivers with equilibrium banks and mobile gravel beds (e.g. Paola and Mohrig, 1996; Parker, 1978), which are likely applicable to the unconsolidated regolith of Mars. The shear stress is a function of flow density (ρ), gravity (g), flow depth (h), and bed slope (s):

$$\tau = \rho g h s \tag{1}$$

Non-dimensionalizing this relationship sets the Shields parameter (θ) equal to 1.2 times the critical Shields number (θ_{cr}), in which the Shields parameter (θ) is defined as:

$$\theta = \frac{\tau}{(\rho_s - \rho) g D_{50}} \tag{2}$$

where ρ_s is sediment density. Using a critical Shields (θ_{cr}) value of 0.03, which is applicable for gravel bed rivers (e.g. Kleinhans and Van den Berg, 2011), and the relative submerged density (R)

$$R = \frac{\rho_s - \rho}{\rho} \tag{3}$$

with a sediment density (ρ_s) value of 3400 kg/m^3 for Martian basaltic rock and a flow density (ρ) value of 1000 kg/m^3, the following depth equation is derived

$$h = 1.2\frac{0.03 D_{50} R}{s}. \tag{4}$$

Flow depths of 3–10 m resulted from Eq. (4). The range in probable flow depths that resulted from both methods agrees well with the few measured values of interior channel depths described above (Hauber et al., 2008; Jaumann et al., 2005).

Table 3
Input variables and results for formation timescales of the Martian valley networks.

Valley network	Volume V (m^3)	Channel width, w (m)	Slope, s (m/m)	Flow depth,[a] h (m) calc. deep	Flow velocity, u (m/s) calc. deep	Flow discharge, Q_f (m^3/s) calc. deep	Sediment discharge, Q_s (m^3/s) calc. deep	Runoff rate, Q_f /A (cm/day) calc. deep	Intermittent formation timescales,[b] T_i (yr) calc. deep		
									Rib.	MPM	van Rijn
12°S, 12°E Evros;	9.6×10^{12}	2330	0.0031	3	1	7×10^{3}	0.6	0.4	9×10^{6}	1×10^{7}	9×10^{7}
				40	8	7×10^{5}	500	42	1×10^{4}	3×10^{4}	2×10^{4}
7°S, 3°E	7.2×10^{11}	1460	0.0009	10	1	2×10^{4}	0.3	4	1×10^{6}	2×10^{6}	1×10^{7}
				25	3	1×10^{5}	10	6	4×10^{4}	7×10^{4}	2×10^{5}
3°S, 5°E	2.8×10^{11}	1950	0.0015	6	1	1×10^{4}	0.4	3	4×10^{5}	5×10^{5}	4×10^{6}
				34	5	3×10^{5}	76	63	2×10^{3}	4×10^{3}	5×10^{3}
0°N, 23°E	1.5×10^{12}	1820	0.0009	10	1	3×10^{4}	4	5	2×10^{6}	3×10^{6}	2×10^{7}
				31	4	2×10^{5}	20	40	4×10^{4}	8×10^{4}	1×10^{5}
2°N, 34°E Naktong west;	4.8×10^{11}	1400	0.0017	5	1	8×10^{3}	0.2	3	2×10^{6}	2×10^{6}	2×10^{7}
				24	4	1×10^{5}	35	53	8×10^{3}	2×10^{4}	2×10^{4}
2°N, 34°E Naktong east;	8.0×10^{12}	1400	0.0012	7	1	1×10^{4}	0.1	0.5	3×10^{7}	4×10^{7}	4×10^{8}
				24	3	1×10^{5}	16	4	3×10^{5}	5×10^{5}	9×10^{5}
12°N, 43°E	1.7×10^{12}	1820	0.0022	4	1	8×10^{3}	0.3	0.9	3×10^{6}	4×10^{6}	4×10^{7}
				31	5	3×10^{5}	130	38	8×10^{3}	2×10^{4}	2×10^{4}
6°S, 45°E	2.1×10^{12}	1820	0.0011	8	1	2×10^{4}	0.3	3	4×10^{6}	5×10^{6}	4×10^{7}
				31	4	2×10^{5}	31	39	4×10^{4}	7×10^{4}	1×10^{5}
Batha River, Africa	6.5×10^{12}	1480	0.0004	7	4	4×10^{4}	4	6	1×10^{6}	4×10^{6}	1×10^{6}

[a] Calculated flow depths were determined using Eq. (4). Deep flow depths were determined from the widths of channels interior to the valleys and a width-to-depth ratio of 58.
[b] Intermittent formation timescale results for each of the three models: Rib (Ribberink, 1998), MPM (Wong and Parker, 2006), and van Rijn (1984a). The Martian results assume valley-incising storms were occurring 5% of the time, as is typical for Earth (Wolman and Miller, 1960). However, the Batha River experiences bankfull discharge for approximately four days out of the year (Schick, 1988), so the Batha results reflect an intermittency of 1%. Continuous formation timescales can be determined by dividing the Martian intermittent formation timescale by 20 or the Batha River intermittent formation timescales by 100.

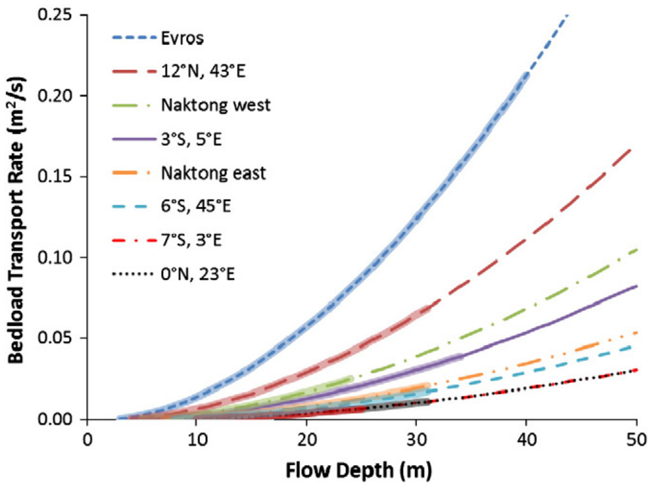

Fig. 3. Bed load sediment transport rates (q_b) for each valley network show a range in values that are a reflection of differences in slope between these valley networks and that are strongly dependent on flow depth. The average values of the three transport models (Section 2.4) are used here. Highlighted ranges in each curve correspond to probable flow depths, as discussed in Section 2.3.

2.4. Flow velocity and sediment transport models

The Darcy–Weisbach (D–W) equation for depth- and width-averaged flow velocity (u) maintains a dependence on the acceleration due to gravity (g) and uses a friction factor (f) to describe the effect of bed roughness on the flow. The D–W equation (Silberman et al., 1963), used herein to calculate average flow velocity (u), is given by:

$$u = \sqrt{\frac{8ghs}{f}}. \tag{5}$$

Since the Martian interior channels are much wider than they are deep, as is typical of terrestrial rivers, the flow depth (h) is used in Eq. (5) as a simplification of the hydraulic radius, $hw/(w+2\,h)$.

The friction factor (f) is often expressed as a function of the relative roughness of the bed (h/D) and incorporates the effect of turbulence, bed forms, and sediment-flow interactions on flow velocity. There is a wide range of D–W friction factors that have been developed for terrestrial flows and applied to Martian conditions (e.g. Kleinhans, 2005; Komar, 1979; Wilson et al., 2004), and their predicted roughness varies considerably (Kleinhans, 2005). However, for the relative roughness typical of these Martian flows (~10^2), the various friction factors (as described in Kleinhans, 2005 and Wilson et al., 2004) produce very similar results with differences well below the level of uncertainty in the calculations. For this work, we use the White–Colebrook function (Silberman et al., 1963).

$$\sqrt{\frac{8}{f}} = 5.74\log_{10}\left(\frac{h}{k_s}\right) + 1.0864 \tag{6}$$

Here, the Nikuradse roughness length (k_s) is taken as being equal to D_{90}, or 0.6 m (Kleinhans, 2005).

The equations that describe sediment transport only deal with the transport of material where grains of sand and rock are sitting on the river bed ready to be moved downstream (transport-limited); they do not reflect the time and energy needed to break up the surface into transportable pieces (erosion-limited). Since these valley networks formed on a substrate that had recently experienced heavy bombardment by impactors, the surface is expected to have had a kilometer or more of unconsolidated, poorly sorted regolith (e.g. Baker and Partridge, 1986; Hartmann and Neukum, 2001), suggesting they formed in transport-limited conditions. Further, when bedrock was exposed, the material transported through bedload processes (i.e. saltating) would act to break up the surface into additional transportable pieces, depending on sediment supply and transport capacity (Sklar and Dietrich, 2004). To account for variations between sediment transport models, which often produce results that are orders of magnitude apart (e.g. Gomez and Church, 1989; Kleinhans, 2005), we compare the results from three models to provide likely timescales of formation. These include models by Ribberink (1998), Meyer-Peter and Mueller (Wong and Parker, 2006) and van Rijn (1984a), which were chosen for their applicability to larger grain bed rivers, their independence on the choice of roughness length (k_s), and their physics-based formulation that minimizes empirical approximations. The sediment transport rates for bed load (q_b) and suspended load (q_s) are often given in non-dimensional form by

$$\varphi_{b,s} = \frac{q_{b,s}}{(Rg)^{1/2} D_{50}{}^{3/2}}. \tag{7}$$

To determine the rate of sediment transport through bedload processes, van Rijn (1984a) solved equations of motion for individual particles within a flow and used experiments of gravel-sized particles to calibrate the model. The van Rijn (1984a) equation for bed load (ϕ_b) transport is a function of the Shields parameter (θ) and non-dimensionalized grain size (D^*):

$$\phi_b = 0.053\left(\frac{\theta - \theta_{cr}}{\theta_{cr}}\right)^{2.1} D_*{}^{-0.3} \tag{8}$$

for which the median grain size is non-dimensionalized with the relative submerged density (R), gravity (g), and kinematic viscosity (ν):

$$D_* = D_{50}\left(\frac{Rg}{\nu^2}\right)^{1/3}. \tag{9}$$

Using the bed shear stress in Eq. (1) to determine the Shields parameter rather than a grain-related shear stress can be done if the river bed had no dunes or other bed forms present. Eq. (1) is preferred over calculating a grain-related shear stress as the latter requires additional use of empirical approximations. The assumption of a plane bed can be supported by conditions at or near those for incipient motion, which is particularly true for the shallower flow depths in each model. All of our model scenarios, however, have Froude numbers less than that for plane bed conditions, placing them in the subcritical flow regime, similar to many terrestrial rivers. Use of the shear stress in Eq. (1) may therefore overestimate the rate of sediment transport, leading to minimum formation timescale results.

The Ribberink (1998) equation for bed load sediment transport was calibrated using a large amount of terrestrial data from a variety of flow regimes, flow velocities, and grain diameters, making it a good choice for modeling sediment transport on Mars (Kleinhans, 2005). The Ribberink (1998) equation is given as:

$$\varphi_b = 11(\theta - \theta_{cr})^{1.65}. \tag{10}$$

The Meyer-Peter and Muller (1948) equation for bedload transport, which is commonly used in terrestrial applications, was reanalyzed by Wong and Parker (2006). They found that by removing an unnecessary bed roughness correction and improving the treatment of boundary shear stress due to side wall effects, the revised Meyer-Peter and Mueller equation better represents bedload transport (Wong and Parker, 2006). This equation is given as

$$\varphi_b = 3.97(\theta - \theta_{cr})^{1.5}. \tag{11}$$

The equations for sediment transport are strongly dependent on flow depth and grain size, both of which have large uncertainties with application to ancient Martian flows. With median grain sizes of 0.1 m and flow depths of 1–50 m, sediment transport within these Martian valley networks occurred primarily through bedload processes rather than suspended by turbulence within the flow. This is similar to sediment transport modeling of Martian delta formation (e.g. Kleinhans et al., 2010). Even for the deepest flows (50 m), which correspond to the fastest flow velocities, we calculate that bed load transport contributes at least one order of magnitude more to the total flux of sediment than suspended load transport. This is confirmed with the high Rouse numbers (greater than 3.2 in all cases) that indicate the settling velocities are many times greater than the shear velocities for all flow depths within each valley network, and therefore that the 0.1 m grains would not have been suspended by these flows. Therefore, suspended load calculations (e.g. van Rijn, 1984b) have not been included in the formation timescales described below.

2.5. Valley network formation timescales

Calculating the sediment discharge (Q_s) as a function of the bed load transport rate (q_b) across the width (w) of the channel can be done by:

$$Q_s = q_b w \tag{12}$$

whereas flow discharge (Q_f) is calculated by:

$$Q_f = hwu. \tag{13}$$

To estimate the duration of time (T) for a valley network to form, the total volume of sediment (V_s) is compared with the rate of sediment transport across the channel (Eq. 13) through the equation (Kleinhans, 2005):

$$T = \frac{V_s}{(1-\lambda)Q_s}. \tag{14}$$

A value of 0.3 (Kleinhans, 2005) is used for the average porosity (λ) of the transported material. This method assumes no additional sediment sources or sinks than what is represented by the current measurable volume within the valleys. If additional sediment was added to the system through aeolian transport or upslope supply (and not visible as an incised valley either due to a resistant surface layer or subsequent infilling), the formation timescales would be longer. Additionally, if these systems were at times erosion-limited, or if their beds experienced armoring as smaller grains were carried downstream leaving a resistive layer of larger grains behind, the transportability of the sediment would be decreased and the formation timescales would be increased. Therefore, these results reflect the minimum amount of flow needed to form the valley networks and, accordingly, the minimum formation timescales.

3. Results and discussion

The valley network specific depth- and width-averaged flow velocities vary between 1 and 8 m/s, depending on flow depth and valley network (Table 3). These velocities are comparable to flow velocities in many terrestrial rivers, including many natural rivers with average velocities between 0.5 and 1.5 m/s (Kleinhans and Van den Berg, 2011), and faster rivers that, depending on the depth of flow, which is often controlled by dam releases, can vary between a few m/s to ten or more m/s (e.g. Graf, 1995; Konieczki et al., 1997). The sediment transport rates on Mars (Fig. 3) increase with flow velocity and result in formation timescales for the eight valley networks in this study that range from about 10^3 yr to 10^8 yr, depending on the valley network and the combination of parameters used (Fig. 4, Table 3).

Exploring the parameter space in these models helps to illustrate the effect many of the variables have on our results, as is shown in Fig. 5 with formation timescale results for Evros Vallis averaged from the three sediment transport models. Grain size (Fig. 5A), which provides some of the greatest uncertainty in these calculations (Kleinhans, 2005), has a significant effect in the resulting formation timescales. If the median grain sizes were smaller than the 0.1 m rocks used in this work that are based on analyses of lander rock size measurements (Kleinhans, 2005), formation timescales would be shorter. Additionally, bedload transport would occur at smaller flow depths and suspended load transport would contribute to an increased transport rate until the system was no longer transport-limited, further decreasing formation timescales. Slope (Figs. 3 and 5B) also has a strong influence on formation timescales, with the steeper slopes facilitating the transport of material downstream and carving out the valleys in shorter time. Changes in flow width (Fig. 5C) have a linear effect on formation timescales (combining Eqs. 12 and 14). Varying width by one or two standard deviations affects the formation timescales by the same factor, which is relatively small compared to the larger uncertainty in grain size and flow depth. Nonetheless, its use in estimating flow depths and runoff rates for these networks makes it an important variable. Bed porosity (Fig. 5D) has only a minor effect on formation timescales. Increasing the flow density (Fig. 5E) to account for salinity had a negligible impact on bed load sediment transport and formation timescales, though sediment density differences between granite (2700 kg/m^3) and Martian basalt (3400 kg/m^3) has as much of an effect on formation timescales as does differences in surface gravity (Fig. 5F). Perhaps more importantly in the low flow depth scenarios where conditions are near that for the beginning of motion, the combination of grain density (Fig. 5E), grain size (Fig. 5A), bed slope (Fig. 5B), and critical shields parameter (Fig. 5 G) all affect the minimum depth at which sediment is transported. Although differences in the acceleration due to gravity between Earth, Mars, or even Titan (Fig. 5F) have an important effect on sediment transport, it is not by itself the most significant variable that changes when applying terrestrial sediment transport equations to flow on other planets.

These methods were also applied to terrestrial river valleys in arid environments to test the validity of the results and our underlying assumption that the Martian valley network formation timescale can be determined by the amount of time it took to transport the sediment out of the drainage basin (i.e. transport-limited). Since terrestrial rivers differ greatly from the ancient Martian valley networks (Carr and Chuang, 1997) due to the influences of vegetation and civilization on water supply, channel incision, and sediment transport, as well as their current active state, and presumably different climatic and tectonic conditions than what Martian valley networks experienced, we applied these same techniques to ephemeral terrestrial rivers so as to minimize these differences. Using Shuttle Radar Topography Mission topographic data (Farr et al., 2007) and Landsat GLS 2005 images (USGS and NASA, 2009) we calculated formation timescales for the African Batha River in the Sahara Desert, Chad. The Chad basin likely experienced alternating periods of aridity and heavy rainfall in response to changing global ice coverage since its formation when the surrounding region experienced uplift approximately 25 million yr ago (Burke, 1976). Assuming median grain sizes of 1 mm (sand) with a density of 2650 kg/m^3; using measured volume (7×10^{12} m^3), slope (0.0004), width (1480 m), and terrace height (7 m) values; treating the porosity (0.3) the same as for the Martian valley network cases; and assuming intermittent formation with flows occurring 4 days out of the year (Schick, 1988), formation timescales for the Batha River were calculated to be 5×10^6 to 2×10^7 yr. With the smaller grain sizes used in these calculations and suspended

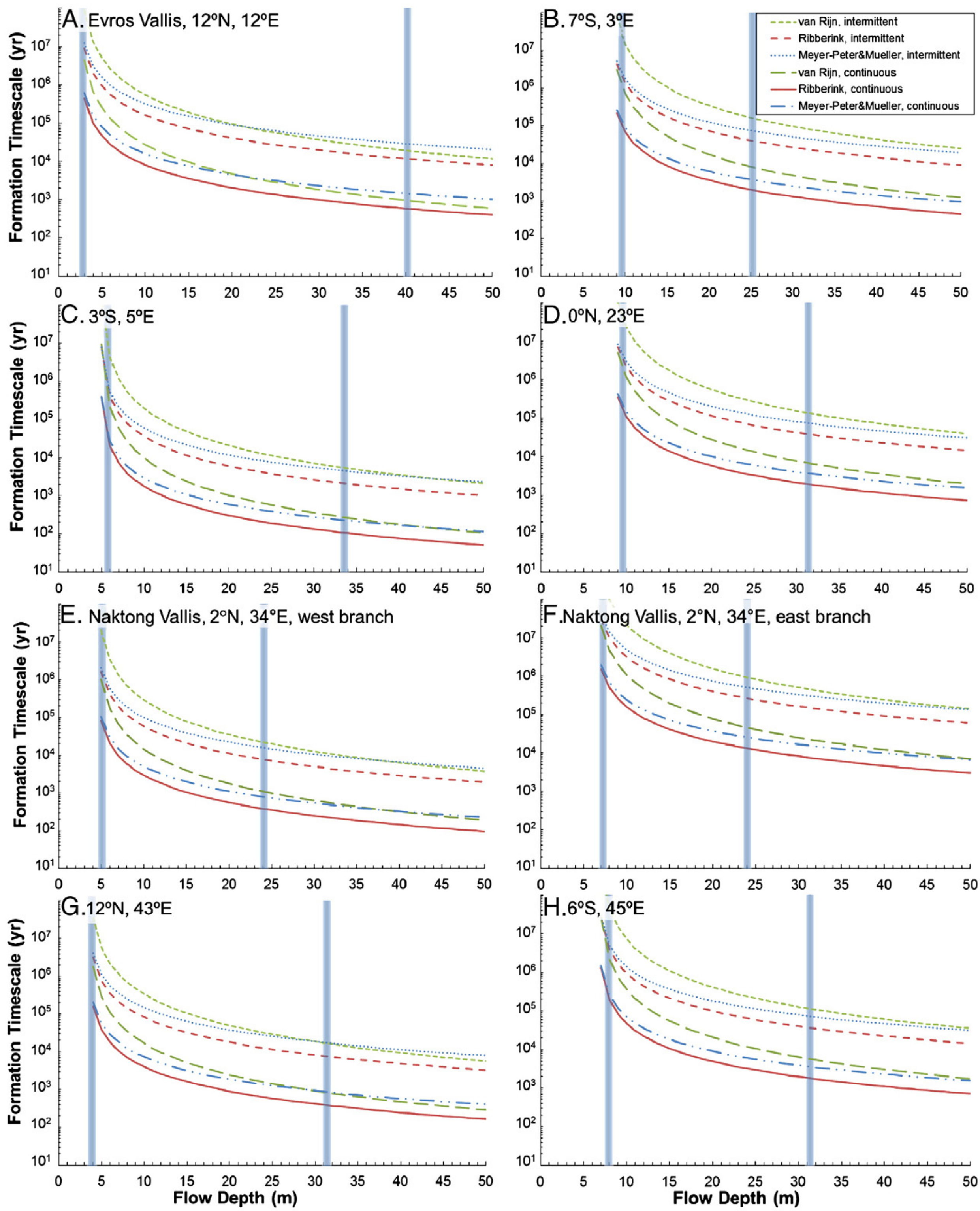

Fig. 4. Formation timescale results for each valley network are given, including both continuous and intermittent results for the Ribberink (1998), Meyer-Peter and Mueller (Wong and Parker, 2006) and van Rijn (1984a) models. Shaded vertical lines correspond to estimated flow depths (Section 2.3, Table 3) that highlight probable formation conditions.

load transport rates comparable to bedload transport rates, formation timescales that incorporate both bed load and suspended load transport are reduced to approximately 4×10^6 yr. Given the complexity in terrestrial climate and tectonic histories and the simplifications we have assumed in this analysis so as to make them applicable to Martian conditions, calculating a formation timescale for the Batha River that is within an order of magnitude of the age of that basin (Burke, 1976) gives confidence to the application of these methods to Martian valley networks.

Table 3 provides estimated runoff rates (Q_f/A) at the network outlet for shallow and deep flow depths for all the Martian valley networks in this study. Any contribution from groundwater sapping or other sources is assumed to be minimal as these valley networks are all interpreted to have formed primarily by precipitation (e.g.

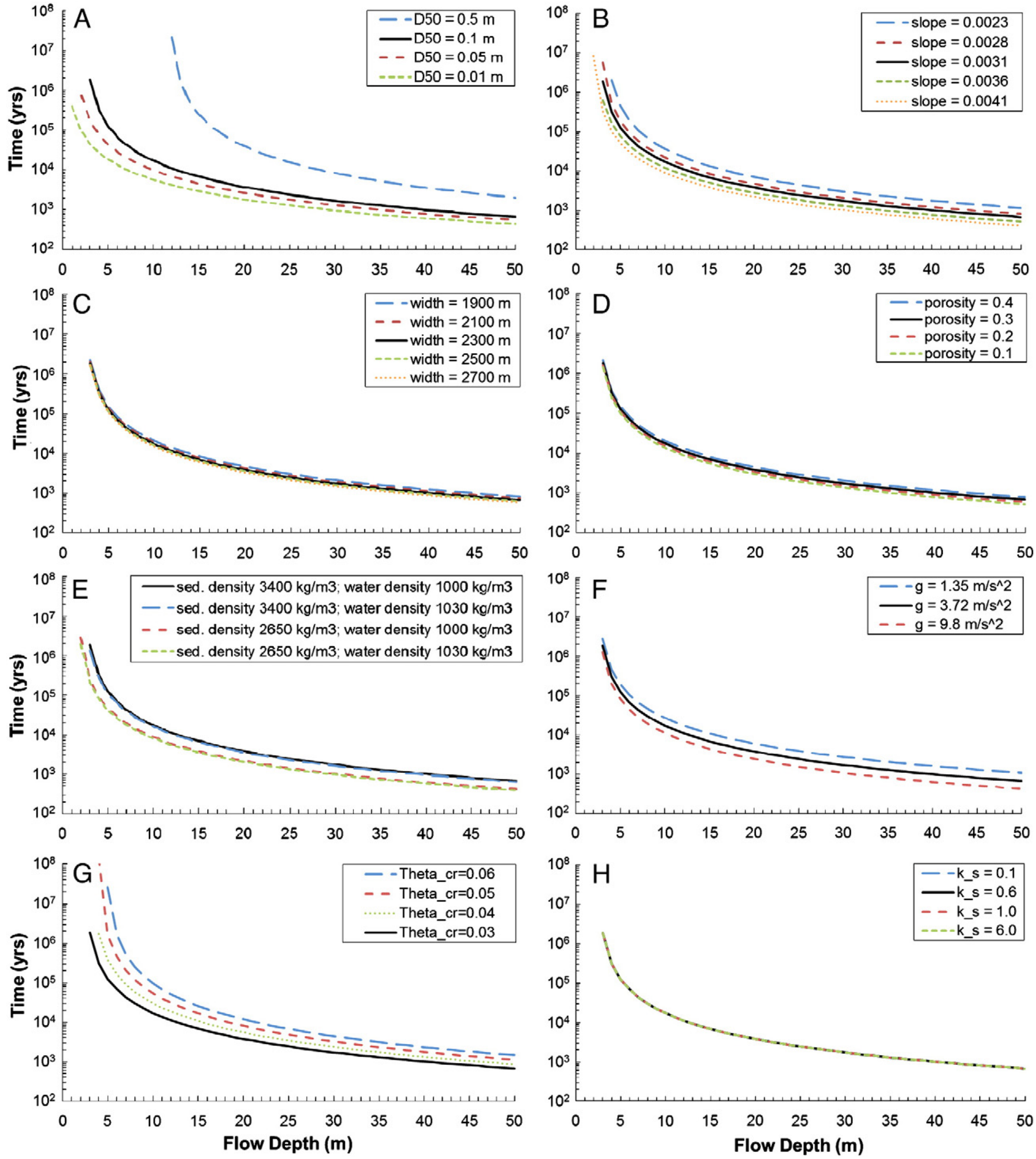

Fig. 5. The effect of key variables on the formation timescale results are shown here. All plots use the average formation timescale results of the three models (Section 2.4) for continuous formation within Evros Vallis. The measured and/or preferred combination of variables (Tables 2 and 3) is indicated by the solid black line. A) Though median grain size (D_{50}) has an uncertainty of one order of magnitude, it is varied here from 0.01 m to 0.5 m due to the interpretation that this is more likely an over estimate than an underestimate of the median grain size at the time of valley formation. B) Slope and C) width values are incremented by +/− one and two standard deviations of their average measured values. D) Bed porosity (λ) varies between 0.1 and 0.4 in Eq. (14). E) Sediment density (ρ_s) is varied between that for sandstone (2650 kg/m^3) and Martian basalt (3400 kg/m^3), and water density (ρ) is varied from pure water (1000 kg/m^3) to increased salinity (1030 kg/m^3). F) Equatorial surface gravity values include those for Earth, Mars, and Titan. G) The critical Shields parameter (θ_{cr}), which determines the minimum shear stress required for sediment transport, usually varies between 0.03 and 0.06. H) The sediment transport models are all independent on choice of Nikuradse roughness length (k_s).

Craddock and Howard, 2002; Hoke and Hynek, 2009; Howard et al., 2005; Hynek and Phillips, 2003), and therefore these runoff rates can be used to approximate precipitation rates over the valley networks. The smaller runoff rates of 0.4–6 cm/day are similar to intense rainfall events that quickly produce flooding in desert regions on Earth (e.g. Coppus and Imeson, 2002; Schick, 1988) and correspond primarily to the shallower flow depth scenarios for each valley network. Two exceptions are the relatively low runoff rates of 6 cm/day and 4 cm/day that occur with the deeper flow depths of 7°S, 3°E (25 m) and the east branch of Naktong Vallis (24 m), respectively. The higher runoff rates of 38–63 cm/day, which approach hurricane conditions on Earth, all occur with deeper flows. If the valley networks formed in arid environments (e.g. Barnhart et al., 2009; Irwin et al., 2011; Stepinski and Stepinski, 2005) in which there were higher infiltration rates and significant evaporation reducing the amount of runoff reaching the mouth of the valley network, the corresponding precipitation rates would have needed to be even greater to produce the calculated runoff rates at the network outlet. Due to the rareness of crater breaches (Barnhart et al., 2009) and the morphology of the valleys and their surrounding terrain that identify precipitation and surface runoff as the primary formation mechanism, it is not expected that the Late Noachian and Early Hesperian were characterized by the extreme runoff rates many of our deeper flow depths require. Therefore, these results suggest that many of the shallower flow depths may be more realistic than the deeper scenarios, and the corresponding longer formation timescales of 10^5 to 10^8 yr (Table 3 and Fig. 4) better represent the period(s) of climate conditions conducive to precipitation during the Late Noachian and Early Hesperian.

This interpretation agrees with the results of landform evolution modeling by Barnhart et al. (2009) and Howard (2007), who found that runoff and evaporation rates in the Late Noachian and Early Hesperian resembled those in arid to semi-arid regions on Earth, characterized by numerous and repeated moderate floods separated by periods of evaporation. Barnhart et al. (2009), who modeled the formation of Parana Vallis, a valley network system that is similar in size and age to the valley networks analyzed in this work (Hoke and Hynek, 2009), found that repeated episodic flows with interim evaporation corresponded to formation timescales of 10^5–10^6 yr for that valley network.

The formation timescales we have determined for these large valley networks are significantly longer than formation timescales that have been calculated for Martian deltas, which often range from days to hundreds of years depending on the delta and methods used (e.g. Hauber et al., 2008; Kleinhans et al., 2010; Kraal et al., 2008). This difference in formation timescale is not surprising due to the steep channel slopes, smaller delta volumes, and at times extremely large flow depths (up to 100 m) that produce delta formation on such short timescales (e.g. Hauber et al., 2008; Kleinhans et al., 2010; Kraal et al., 2008).

The hypothesis that the Martian valley networks formed during periods of climate change caused primarily by impact events early in Martian history (e.g. Segura et al., 2008) is not supported by the results of this nor other work (e.g. Fassett and Head, 2008b, 2011; Hynek et al., 2010). Contrary to the arguments in Toon et al. (2010) that the timing of the impact events (Werner, 2008) coincided with the timing of valley network formation (Fassett and Head, 2008b), hundreds of millions of years span the formation of most of the large impacts (3.9–4.1 Ga) and the formation of most of the large (by total valley length) valley networks (none older than 3.8 Ga), with the possible exception of a few younger, smaller impact basins (e.g. Antoniadi, and Lowell) and some older, smaller valley networks. The greatest degree of valley incision, which presumably coincides with the greatest degree of precipitation and surface runoff (e.g. Irwin et al., 2011), occurred at least 100 to 200 million yr after the impact-related climate change described by Segura et al. (2008). Since each impact event produced only a few centuries, at best, of active hydrological cycles and precipitation, the timing of valley incision and impact-related climate change cannot be considered contemporaneous.

Further, all of the valley networks in this study require several orders of magnitude longer durations of clement conditions to form than can be provided by the impact events, even considering unrealistic scenarios of continuously high runoff rates. So although a few impact basins may have formed during the time of large valley network formation, the few tens to hundreds of years of precipitation related to those events, whether continuous or intermittent, is insufficient to form these large valley networks.

Comparing the formation timescales of each valley network with their corresponding crater ages suggest the precipitation that produced flows of sufficient magnitude to allow bed load transport and incision of the large valley networks was 1) limited to the Late Noachian and Early Hesperian, as many others have suggested (e.g. Howard et al., 2005; Hynek and Phillips, 2001; Irwin et al., 2005a, 2011), 2) did not happen simultaneously across the planet, and 3) lasted intermittently for periods of 10^5 to 10^6 yr. For example, the east and west branches of Naktong Vallis exhibit different preservation states and distinctly different crater populations, suggesting the east branch is overall younger than the west branch (Hoke and Hynek, 2009). Comparing their formation timescales shows that the west branch (and likely part of the east branch) formed about 3.79 Ga with possible runoff rates of >3 cm/day lasting intermittently for 10^5–10^7 yr (Fig. 6). Then, 60–90 million yr later when intense precipitation returned to this region, it was focused to the south and east over the more densely dendritic part of the east branch and its neighbor at 6°S, 45°E (Fig. 1). These valley networks share similar crater ages as their neighbors at 12°N, 45°E and 0°N, 23°E, placing their formation together at approximately 3.70–3.73 Ga (Hoke and Hynek, 2009). Assuming the duration of formation was about the same order of magnitude for these neighboring valley networks, precipitation likely occurred intermittently for 10^6–10^7 yr, with runoff rates of 1–3 cm/day across Naktong Vallis, 1–2 cm/day at 12°N, 43°E, >4 cm/day at 6°S, 45°E, and >5 cm/day at 0°N, 23°E (Fig. 6). Likewise, the three proximal valley networks located to the southeast of Meridiani Planum (Fig. 1) all have crater ages that place their formation coevally around 3.63 to 3.65 Ga (Hoke and Hynek, 2009), approximately 60–80 million yr after Naktong Vallis and its neighbors finished forming. Assuming these valley networks near Meridiani Planum experienced approximately the same duration of precipitation as each other, it is likely these valley networks formed with intermittent runoff rates of 1–9 cm/day, lasting 10^5–10^7 yr (Fig. 6).

However, given the large uncertainty of these results and the choice of parameters that led to these timescales being minimum values, these results do not exclude the possibility that there may have been some overlap in formation episodes. Either way, regions not actively incising may have been extremely arid, or, more likely, may have experienced minor precipitation in amounts too low to support sediment transport and valley incision, as has been suggested for much of Martian history prior to the Noachian–Hesperian boundary and incision of most of the valley networks (Irwin et al., 2011). If this were the case, as Mars was becoming more arid toward the end of this final epoch of intense fluvial erosion in the Late Noachian, valley formation was also likely changing. On Earth, climate change toward increasing aridity can potentially increase erosion rates despite a decrease in the frequency of precipitation events and overall river discharge (e.g. Molnar, 2001; Tucker et al., 2006). We expect that valley networks that formed toward the end of this period of fluvial erosion may have been characterized by less frequent, more intense storms. This is supported by the relatively shorter formation timescales (factor of 10 less) for the valley networks that formed later (Meridiani group) than those that formed earlier (Naktong group).

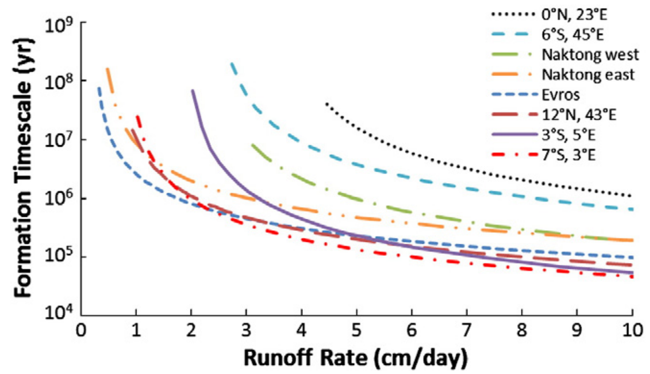

Fig. 6. Comparing the runoff rates (cm/day) with the corresponding formation timescale (years) for each valley network helps constrain possible formation scenarios.

4. Conclusion

Comparing the formation timescales of the valley networks analyzed in this work to their crater density-derived ages (Hoke and Hynek, 2009) reveals an early Martian climate characterized by many periods of increased precipitation and valley incision, each lasting 10^5–10^7 yr, over the 10^8 yr of valley formation. Though, considering the large uncertainty in these calculations and the combination of parameters that produced minimum timescales, it is possible that the formation timescales approach durations similar to their span in ages. Valley networks often share similar ages and formation timescales as their neighboring networks, consistent with regional weather patterns delivering precipitation of sufficient magnitude to form the valleys while other non-incising regions receive minor precipitation, if any. Regardless, the amount of time required to form these large valley networks does not extend valley formation to earlier than the Late Noachian and is consistent with hypotheses that valley incision was constrained to a relatively short period of Martian history near the Noachian–Hesperian boundary (e.g. Howard et al., 2005; Hynek and Phillips, 2001; Irwin et al., 2005a, 2011).

Acknowledgments

We appreciate the helpful advice on calculating volume within the valley networks and other constructive discussions with Gaetano Di Achille early in this project. Constructive reviews by Maarten Kleinhans and an anonymous reviewer greatly improved the final manuscript. This work was funded by NASA Mars Data Analysis Award NNX06AE08G.

References

Baker, V.R., Partridge, J.B., 1986. Small Martian valleys: pristine and degraded morphology. J. Geophys. Res. 91, 3561–3572. doi:10.1029/JB091iB03p03561.
Barnhart, C.J., Howard, A.D., Moore, J.M., 2009. Long-term precipitation and late-stage valley network formation: landform simulations of Parana Basin. Mars. J. Geophys. Res. 114. doi:10.1029/2008JE003122.
Bjerklie, D.M., Dingman, S.L., Vorosmarty, C.J., Bolster, C.H., Congalton, R.G., 2003. Evaluating the potential for measuring river discharge from space. J. Hydrol. 278, 17–38. doi:10.1016/S0022-1694(03)00129-X.
Burke, K., 1976. The Chad Basin: an active intra-continental basin. Tectonophysics 36, 197–206.
Carr, M.H., 1996. Water on Mars. Oxford University Press, New York. 229 p.
Carr, M.H., Chuang, F.C., 1997. Martian drainage densities. J. Geophys. Res. 102, 9145–9152.
Carr, M.H., Malin, M.C., 2000. Meter-scale characteristics of Martian channels and valleys. Icarus 146, 366–386.
Christensen, P.R., 1986. Regional dust deposits on Mars: physical properties, age, and history. J. Geophys. Res. 91, 3533–3545. doi:10.1029/JB091iB03p03533.
Christensen, P.R., Jakosky, B.M., Kieffer, H.H., Malin, M.C., McSween, H.Y., Nealson, K., Mehall, G.L., Silverman, S.H., Ferry, S., Caplinger, M., Ravine, M., 2004. The Thermal Emission Imaging System (THEMIS) for the Mars 2001 Odyssey Mission. Space Sci. Rev. 110, 85–130.
Coppus, R., Imeson, A.C., 2002. Extreme events controlling erosion and sediment transport in a semi-arid sub-andean valley. Earth Surf. Process. Landforms 27, 1365–1375. doi:10.1002/esp. 435.
Craddock, R.A., Howard, A.D., 2002. The case for rainfall on a warm, wet early Mars. J. Geophys. Res. 107 (Ell), 5111.
Di Achille, G., Hynek, B.M., 2010. Ancient ocean on Mars supported by global distribution of deltas and valleys. Nat. Geosci. 3. doi:10.1038/NGEO891.
Farr, T.G., Rosen, P.A., Caro, E., et al., 2007. The Shuttle Radar Topography Mission. Rev. Geophys. 45, RG2004. doi:10.1029/2005RG000183.
Fassett, C.I., Head III, J.W., 2008a. Valley network-fed, open-basin lakes on Mars: distribution and implications for Noachian surface and subsurface hydrology. Icarus 198, 37–56. doi:10.1016/j.icarus.2008.06.016.
Fassett, C.I., Head III, J.W., 2008b. The timing of Martian valley network activity: constraints from buffered crater counting. Icarus 195, 61–89. doi:10.1016/j.icarus.2007.12.009.
Fassett, C.I., Head, J.W., 2011. Sequence and timing of conditions on early Mars. Icarus 211, 1204–1214. doi:10.1016/j.icarus.2010.11.014.
Fenton, L.K., Bandfield, J.L., Ward, A.W., 2003. Aeolian processes in Proctor Crater on Mars: sedimentary history as analyzed from multiple data sets. J. Geophys. Res. 108 (E12), 5129. doi:10.1029/2002JE002015.
Finnegan, N.J., Roe, G., Montgomery, D.R., Hallet, B., 2005. Controls on the channel width of rivers: implications for modeling fluvial incision of bedrock. Geology 33, 229–232. doi:10.1130/G21171.1.
Gioia, G., Bombardelli, F.A., 2002. Scaling and similarity in rough channel flows. Phys. Rev. Lett. 88. doi:10.1103/PhysRevLett88.014501.
Goldspiel, J.M., Squyres, S.W., 1991. Ancient aqueous sedimentation on Mars. Icarus 89, 392–410.
Golombek, M., Rapp, D., 1997. Size-frequency distribution of rocks on Mars and Earth analog sites: implications for future landed missions. J. Geophys. Res. 102 (E2), 4117–4129.
Golombek, M.P., Haldermann, A.F.C., Forsberg-Taylor, N.K., DiMaggio, E.N., Schroeder, R.D., Jakosky, B.M., Mellon, M.T., Matijevic, J.R., 2003. Rock size-frequency distributions on Mars and implications for Mars Exploration Rover landing safety and operations. J. Geophys. Res. 108 (E12), 8086. doi:10.1029/2002JE002035.
Golombek, M.P., Arvidson, R.E., Bell III, J.F., Christensen, P.R., Crisp, J.A., Crumpler, L.S., Ehlmann, B.L., Fergason, R.L., Grant, J.A., Greeley, R., Haldemann, A.F.C., Kass, D.M., Parker, T.J., Schofield, J.T., Squyres, S.W., Zurek, R.W., 2005. Assessment of Mars Exploration Rover landing site predictions. Nature 436, 44–48. doi:10.1038/nature03600.
Golombek, M.P., Crumpler, L.S., Grant, J.A., Greeley, R., Cabrol, N.A., Parker, T.J., Rice Jr., J.W., Ward, J.G., Arvidson, R.E., Moersch, J.E., Fergason, R.L., Christensen, P.R., Castan, A., Castan, R., Haldemann, A.F.C., Li, R., Bell III, J.F., Squyres, S.W., 2006. Geology of the Gusev cratered plains from the Spirit rover transverse. J. Geophys. Res. 100. doi:10.1029/2005JE002503.
Gomez, B., Church, M., 1989. An assessment of bed load sediment transport formulae for gravel bed rivers. Water Resour. Res. 25, 1161–1186.
Graf, J.B., 1995. Measured and predicted velocity and longitudinal dispersion at steady and unsteady flow, Colorado River, Glen Canyon Dam to Lake Mead. Water Resour. Bull. 31 (2), 265–281.
Hartmann, W.K., Neukum, G., 2001. Cratering chronology and the evolution of Mars. Space Sci. Rev. 96, 165–194. doi:10.1023/A:1011945222010.
Hauber, E., Gwinner, K., Kleinhans, M., Reiss, D., Di Achille, G., Ori, G.-G., Scholten, F., Marinangeli, L., Jaumann, R., Neukum, G., 2008. Sedimentary deposits in Xanthe Terra: implications for the ancient climate on Mars. Planet. Space Sci. 57, 944–957. doi:10.1016/j.pss.2008.06.009.
Herkenoff, K., Squyres, S.W., Arvidson, R., Bass, D.S., Bell III, J.F., Bertelsen, P., Cabrol, N.A., Gaddis, L., Hayes, A.G., Hviid, S.F., Johnson, J.R., Kinch, K.M., Madsen, M.B., Maki, J.N., McLennan, S.M., McSween, H.Y., Rice Jr., J.W., Sims, M., Smith, P.H., Soderblom, L.A., Spanovich, N., Sullivan, R., Wang, A., 2004. Textures of the soils and rocks at Gusev Crater from Spirit's Microscopic Imager. Science 305, 824–826. doi:10.1126/science.1100015.
Hoke, M.R.T., Hynek, B.M., 2009. Roaming zones of precipitation on ancient Mars as recorded in valley networks. J. Geophys. Res. 114. doi:10.1029/2008JE003247.
Howard, A.D., 2007. Simulating the development of Martian highland landscapes through the interaction of impact cratering, fluvial erosion, and variable hydrologic forcing. Geomorphology 91, 332–363. doi:10.1016/j.geomorph.2007.04.017.
Howard, A.D., Moore, J.M., Irwin III, R.P., 2005. An intense terminal epoch of widespread fluvial activity on early Mars: 1. Valley network incision and associated deposits. J. Geophys. Res. 110, E12S14.
Hynek, B.M., Phillips, R.J., 2001. Evidence for extensive denudation of the Martian highlands. Geology 29, 407–410.
Hynek, B.M., Phillips, R.J., 2003. New data reveal mature, integrated drainage systems on Mars indicative of past precipitation. Geology 31, 757–760.
Hynek, B.M., Beach, M., Hoke, M.R.T., 2010. Updated global map of Martian valley networks and implications for climate and hydrologic processes. J. Geophys. Res. 115. doi:10.1029/2009JE003548.
Irwin III, R.P., Howard, A.D., Craddock, R.A., Moore, J.M., 2005a. An intense terminal epoch of widespread fluvial activity on early Mars. 2. Increased runoff and paleolake development. J. Geophys. Res. 110. doi:10.1029/2005JE002460.
Irwin III, R.P., Craddock, R.A., Howard, A.D., 2005b. Interior channels in Martian valley networks: discharge and runoff production. Geology 33, 489–492. doi:10.1130/G21333.1.
Irwin III, R.P., Craddock, R.A., Howard, A.D., Flemming, H.L., 2011. Topographic influences on development of Martian valley networks. J. Geophys. Res. 116. doi:10.1029/2010JE003620.
Jaumann, R., Reiss, D., Frei, S., Neukum, G., Scholten, F., Gwinner, K., Roatsch, T., Matz, K.-D., Mertens, V., Hauber, E., Hoffmann, H., Kohler, U., Head, J.W., Hiesinger, H., Carr, M.H., 2005. Interior channels in Martian valleys: constraints on fluvial erosion by measurements of the Mars Express High Resolution Stereo Camera. Geophys. Res. Lett. 32. doi:10.1029/2005GL023415.
Jaumann, R., Neukum, G., Behnke, T., Duxbury, T.C., Eichentopf, K., Flohrer, J., van Gasselt, S., Giese, B., Gwinner, K., Hauber, E., Hoffmann, H., Hoffmeister, A., Kohler, U., Matz, K.-D., McCord, T.B., Mertens, V., Oberst, J., Pischel, R., Reiss, D., Ress, E., Roatsch, T., Saiger, P., Scholten, F., Schwarz, G., Stephan, K., Wahlisch, M., the HRSC Co-Investigator Team, 2007. The high-resolution stereo camera (HRSC) experiment on Mars Express: instrument aspects and experiment conduct from interplanetary cruise through the nominal mission: planet. Space Sci. 55, 928–952.
Kleinhans, M.G., 2005. Flow discharge and sediment transport models for estimating a minimum timescale of hydrological activity and channel and delta formation on Mars. J. Geophys. Res. 110, E12003.
Kleinhans, M.G., van de Kasteele, H.E., Hauber, E., 2010. Paleoflow reconstruction from fan delta morphology on Mars. Earth Planet. Sci. Lett. 294, 378–392. doi:10.1016/j.epsl.2009.11.025.
Kleinhans, M.G., Van den Berg, J.H., 2011. River channel and bar patterns explained and predicted by an empirical and physics-based method. Earth Surf. Process. Landforms 36, 721–738. doi:10,1002/esp. 2090.
Komar, P., 1979. Comparisons of the hydraulics of water flows in Martian outflow channels with flows of similar scale on Earth. Icarus 37, 156–181.
Komar, P., 1980. Modes of sediment transport in channelized water flows, with ramifications to the erosion of the Martian outflow channels. Icarus 42, 317–329.

Konieczki, A.D., Graf, J.B., Carpenter, M.C., 1997. Streamflow and sediment data collected to determine the effects of a controlled flood in March and April 1996 on the Colorado River between Lees Ferry and Diamond Creek, Arizona. U. S. Geological Survey Open-File Report 97–224. 55p.

Kraal, E.R., van Dijk, M., Postma, G., Kleinhans, M.G., 2008. Martian stepped-delta formation by rapid water release. Nature 451. doi:10.1038/nature06615.

Malin, M.C., Bell III, J.F., Cantor, B.A., Caplinger, M.A., Calvin, W.M., Clancy, R.T., Edgett, K.S., Edwards, L., Haberle, R.M., James, P.B., Lee, S.W., Ravine, M.A., Thomas, P.C., Wolff, M.J., 2007. Context Camera Investigation on board the Mars Reconnaissance Orbiter. J. Geophys. Res. 112 (E05S04). doi:10.1029/2006JE002808.

Manning, R., 1891. On the flow of water in open channels and pipes. Inst. Civil Eng. Ireland Trans. 20, 161–207.

Meyer-Peter, E., Muller, R., 1948. Formulas for bed-load transport. Proc., 3rd Conf. Int. Association of Hydraulic Research, Stockholm, Sweden, pp. 39–64.

Milton, D.J., 1973. Water and process of degradation in the Martian landscape. J. Geophys. Res. 78 (20), 4037–4047.

Molnar, P., 2001. Climate change, flooding in arid environments, and erosion rates. Geology 29 (12), 1071–1074.

Neukum, G., Jaumann, R., the HRSC Co-Investigator and Experiment Team, 2004. HRSC: The High Resolution Stereo Camera of Mars Express. In: Wilson, A. (Ed.), Mars Express: The Scientific Payload. ESA, Noordwijk, The Netherlands, pp. 17–35.

Osterkamp, W.R., Hedman, E.R., 1982. Perennial-streamflow characteristics related to channel geometry and sediment in Missouri River basin. U. S. Geological Survey Professional Paper, 1242. 37.p.

Paola, C., Mohrig, D., 1996. Palaeohydraulics revisited: palaeoslope estimation in coarse-grained braided rivers. Basin Res. 8, 243–254.

Parker, G., 1978. Self-formed straight rivers with equilibrium banks and mobile bed. Part 2. The gravel river. J. Fluid Mech. 89, 127–146.

Pelkey, S.M., Jakosky, B.M., Mellon, M.T., 2001. Thermal inertia of crater-related wind streaks on Mars. J. Geophys. Res. 106, 23909–23920.

Presley, M.A., Christensen, P.R., 1997. Thermal conductivity measurements of particulate materials 2. Results. J. Geophys. Res. 102, 6551–6566.

Putzig, N.E., Mellon, M.T., 2007. Apparent thermal inertia and the surface heterogeneity of Mars. Icarus 191, 68–94. doi:10.1016/j.icarus.2007.05.013.

Ribberink, J.S., 1998. Bed-load transport for steady flows and unsteady oscillatory flows. Coast. Eng. 34, 59–82.

Schick, A.P., 1988. Hydrologic aspects of floods in extreme arid environments. In: Baker, V.R., Kochel, R.C., Patton, P.C. (Eds.), Flood Geomorphology.

Segura, T.L., Toon, O.B., Colaprete, A., 2008. Modeling the environmental effects of moderate-sized impacts on Mars. J. Geophys. Res. 113, E11007. doi:10.1029/2008JE003147.

Sklar, L.S., Dietrich, W.E., 2004. A mechanistic model for river incision into bedrock by saltating bed load. Water Resour. Res. 40, W06301. doi:10.1029/2003WR002496.

Silberman, E., Carter, R., Einstein, H., Hinds, J., Powell, R., ASCE Task Force on Friction Factors in Open Channels, 1963. Friction factors in open channels. J. Hydraul. Eng. 89, 97–143 HY2.

Smith, D.E., Zuber, M.T., Frey, H.V., et al., 2001. Mars orbiter laser altimeter: experiment summary after the first year of global mapping of Mars. J. Geophys. Res. 106, 23689–23722. doi:10.1029/2000JE001364.

Som, S.M., Montgomery, D.R., Greenberg, H.M., 2009. Scaling relations for large Martian valleys. J. Geophys. Res. 114, E02005. doi:10.1029/2008JE003132.

Squyres, S.W., Arvidson, R.E., Bell, I.I.I., et al., 2004. The Opportunity Rover's Athena Science Investigation at Meridiani Planum, Mars. Science 306, 1698–1703. doi:10.1126/science.1106171.

Stepinski, T.F., Stepinski, A.P., 2005. Morphology of drainage basins as an indicator of climate on early Mars. J. Geophys. Res. 110 (E12S12). doi:10.1029/2005JE002448.

Toon, O.B., Segura, T., Zhanle, K., 2010. The formation of Martian river valleys by impacts. Annu. Rev. Earth Planet. Sci. 38, 303–322. doi:10.1146/annurev-earth-040809-152354.

Tucker, G.E., Arnold, L., Bras, R.L., Flores, H., Istanbulluoglu, E., Solyom, P., 2006. Headwater channel dynamics in semiarid rangelands, Colorado high plains, USA. GSA Bull. 118, 959–974 10.1130B25928.1.

USGS, NASA, 2009. Global Land Survey 2005, Sioux Falls. USGS Center for Earth Resources Observation and Science (EROS), SD USA.

van Rijn, L.C., 1984a. Sediment transport, part I: bed load transport. J. Hydraul. Eng. 110, 1431–1456.

van Rijn, L.C., 1984b. Sediment transport, part II: suspended load transport. J. Hydraul. Eng. 110, 1613–1641.

Werner, S.C., 2008. The early Martian evolution — constraints from basin formation ages. Icarus 195, 45–60. doi:10.1016/j.icarus.2007.12.008.

Wilson, L., Ghatan, G.J., Head III, J.W., Mitchell, K.L., 2004. Mars outflow channels: a reappraisal of the estimation of water flow velocities from water depths, regional slopes, and channel floor properties. J. Geophys. Res. 109, E09003.

Wolman, M.G., Miller, J.P., 1960. Magnitude and frequency of forces in geomorphic process. J. Geol. 68, 54–74.

Wong, M., Parker, G., 2006. Reanalysis and correction of bed-load relation of Meyer-Peter and Muller using their own database. J. Hyrdaul. Eng. 132, 1159–1168. doi:10.1061/(ASCE)0733-9429(2006) 132:11(1159).